RADIO SCIENCE, VOL. 38, NO. 4, 8074, doi:10.1029/2002RS002674, 2003

Cloud model–based Bayesian technique for precipitation profile retrieval from the Tropical Rainfall Measuring Mission Microwave Imager

Alessandra Tassa, Sabatino Di Michele, and Alberto Mugnai

Istituto di Scienze dell'Atmosfera e del Clima, Consiglio Nazionale delle Ricerche, Rome, Italy

Frank S. Marzano

Dipartimento di Ingegneria Elettrica, CETEMPS, Università dell'Aquila, Monteluco di Roio, L'Aquila, Italy

José Pedro V. Poiares Baptista

European Space Research and Technology Centre, European Space Agency, Noordwjik, Netherlands

Received 11 March 2002; revised 6 July 2002; accepted 10 July 2002; published 24 June 2003.

[1] A cloud model–based statistical retrieval technique for estimating surface precipitation and cloud profiles over ocean, called Bayesian Algorithm for Microwave Precipitation Retrieval (BAMPR), is described. The inversion scheme, based on the Bayesian estimation theory, is trained by a CRD obtained by inputting the numerical outputs of a mesoscale microphysical model into a three-dimensional radiative transfer model. Since the performances of the retrieval are strictly dependent on the a priori information given by the CRD, the generation of the database itself, and the coupling between the forward and the inverse problem are carefully discussed. Particular emphasis is given to the database representativeness of the meteorological event under investigation and to the quantification of modeling errors. The retrieval uncertainties are provided with the estimates themselves by choosing the Minimum Mean Square technique as a Bayesian inversion method. As an example, the algorithm is applied to some case studies in the Tropics using the Tropical Rainfall Measuring Mission (TRMM) Microwave Imager data. The analysis is focused on the evaluation of the CRD performances with respect to the various events (i.e., a tropical cyclone, a tropical storm, a summer front, and some isolated convective cells in the Atolls region) and different CRDs (i.e., two hurricanes from the University of Wisconsin Nonhydrostatic Modeling System and a tropical squall line from the Goddard Cumulus Ensemble model). A detailed examination is carried out on the case of the hurricane Bonnie on 25 August 1998, which is discussed by using TRMM official products as a comparison. *INDEX TERMS:* 3360 Meteorology and Atmospheric Dynamics: Remote sensing; 3354 Meteorology and Atmospheric Dynamics: Precipitation (1854); 3359 Meteorology and Atmospheric Dynamics: Radiative processes; *KEYWORDS:* precipitation retrieval, TRMM Microwave Imager, cloud-radiation database

Citation: Tassa, A., S. Di Michele, A. Mugnai, F. S. Marzano, and J. P. V. Poiares Baptista, Cloud model–based Bayesian technique for precipitation profile retrieval from the Tropical Rainfall Measuring Mission Microwave Imager, *Radio Sci.*, *38*(4), 8074, doi:10.1029/2002RS002674, 2003.

1. Introduction

[2] Retrieval of precipitation profiles from spaceborne microwave sensors has received a new attention after the launch of the Tropical Rainfall Measuring Mission (TRMM) platform in 1997 [*Simpson et al.*, 1996; *Kummerow et al.*, 1998]. Several inversion techniques have

0048-6604/03/2002RS002674$11.00

been proposed and applied in the last two decades for estimating cloud and precipitation parameters from measurements taken by spaceborne microwave radiometers; especially, the Special Sensor Microwave/Imagers (SSM/Is) flown aboard spacecrafts of the U.S. Defense Meteorological Satellite Program (DMSP) (see *Smith et al.* [1998] for comprehensive descriptions of several SSM/I algorithms). Among these techniques, we enumerate the approaches on the basis of multiple regression and on Maximum Likelihood methods.

[3] Recently, Bayesian techniques have been proved to have a large potential and flexibility for precipitation profiling [e.g., *Evans et al.*, 1995; *Kummerow et al.*, 1996; *Pierdicca et al.*, 1996; *Marzano et al.*, 1999; *Kummerow et al.*, 2001]. Their unique feature is that they constitute a rigorous statistical framework in which to develop cloud model–based inversion methods and combined multisensor approaches. As opposed to empirical methods, where measurements of both brightness temperatures and precipitation parameters are collected to train a retrieval algorithm, the model-based approaches resort to refined physical models to simulate the measurements [e.g., *Smith et al.*, 1992; *Mugnai et al.*, 1993; *Smith et al.*, 1994; *Kummerow et al.*, 1996]. This point of view offers the possibility to avoid in situ measurements and to deepen the understanding of the problem. On the other hand, model-based approaches have to tackle the critical issue of tuning simulations to the measurement manifolds in order to be representative of real observations [*Panegrossi et al.*, 1998; *Tassa et al.*, 1999].

[4] In this work, we describe the methodological features of the Bayesian Algorithm for Microwave-Based Precipitation Retrieval (BAMPR). The retrieval scheme is trained by three-dimensional (3-D) dynamical cloud-resolving model outputs combined with 3-D radiative transfer models. The description of the algorithm is accomplished in the first part of the paper. The algorithm is intended to address the problem of the physical consistency and adequateness of the retrieval first-guess (i.e., the CRD) and provides a valuable and robust inversion technique for intense meteorological events. As a matter of fact, special attention is devoted to the methodology used for coupling the CRD with the retrieval scheme. In the second part of the paper, some applications of BAMPR to TRMM data are discussed. In particular, the case of the hurricane Bonnie on 25 August 1998 is analyzed and discussed in detail. The estimated precipitation rates are compared with the official TRMM products, both from the radiometer and from the precipitation radar.

2. Bayesian Algorithm for Microwave-Based Precipitation Retrieval

[5] The block diagram of the Bayesian Algorithm for Microwave Precipitation Retrieval (BAMPR) is shown in Figure 1. This algorithm has been developed for using data acquired by the TRMM Microwave Imager (TMI), but a combined version (for active and passive sensor merging) has also been developed, aimed at the exploitation of data from the Precipitation Radar (PR) aboard the TRMM platform [*Marzano et al.*, 2000; *Di Michele et al.*, 2003].

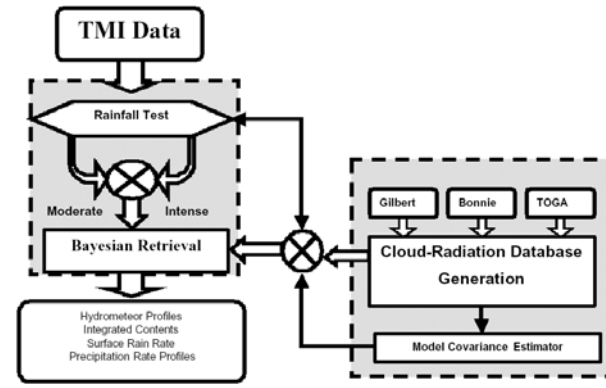

Figure 1. Block diagram of the Bayesian Algorithm for Microwave-Based Precipitation Retrieval (BAMPR) for TMI precipitation profile retrieval. The three blocks "Gilbert," "Bonnie," and "TOGA" refer to the cloud model simulations currently used within BAMPR for tropical applications over ocean.

[6] In Figure 1 the two gray-contoured boxes refer to the two main blocks common to all physically based retrieval approaches [*Mugnai et al.*, 1993; *Smith et al.*, 1994; *Pierdicca et al.*, 1996; *Kummerow et al.*, 1996; *Marzano et al.*, 2000; *Kummerow et al.*, 2001]. They are generally referred to as the "forward problem" and the "inverse problem."

[7] The forward problem, described in section 2.1, consists in the generation of a database (the "cloud radiation database" (CRD)), in which the simulated brightness temperatures (TBs) that would be measured by a spaceborne radiometer are associated with the various cloud structures generated by a cloud-resolving numerical model. The CRD generation block accounts for the simulation of the upwelling TBs corresponding to each cloud structure. In the proposed scheme, we associate to each set of TBs a slanted profile (according to the 53.1° viewing angle of the radiometer) at the resolution of the 37 GHz channels. This association is not straightforward, especially in the case of a 3-D geometry approach as explained later on. Cloud model simulations used in this work are referred to two hurricanes (i.e., Gilbert and Bonnie) from the University of Wisconsin Nonhydrostatic Modeling System and to a tropical squall line (i.e., *TOGA*; *Kummerow et al.* [1996]) from the Goddard Cumulus Ensemble model. The frequency-

dependent model and instrumental errors are evaluated by means of the error covariance estimator module by using ancillary information and numerical sensitivity tests. The output of the forward modeling procedure is the construction of a statistically significant CRD.

[8] In the inverse problem, described in section 2.3, TMI data are ingested to perform a rainfall test in order to distinguish between moderate and intense rainfall classes. This classification is performed using TMI TBs texture information and centroids derived from the CRD itself. The latter is therefore used to train the Bayesian retrieval, whose products are the hydrometeor content profiles (in g/m^3) and the precipitation rate profiles (in mm/h) together with the hydrometeor columnar contents (in kg/m^2) and the surface rain rates (in mm/h). The Bayesian technique has been applied by resorting to the Minimum Mean Square (MMS) criterion.

[9] In what follows, section 2.2 is dedicated to the topic of coupling CRDs and Bayesian techniques. Critical issues, such as data matching and representativeness, are emphasized in order to define an ''optimal'' use of a CRD for inversion purposes.

2.1. The Forward Problem

[10] For the TMI precipitation profile retrieval, the CRD consists of a large set (thousands) of slanted precipitating cloud profiles and of the corresponding brightness temperatures at TMI channels and resolutions, generated as explained in the following.

2.1.1. Cloud Radiation Database Generation

[11] The precipitating cloud structures are based on the outputs of 3-D numerical mesoscale nonhydrostatic cloud-resolving models, which explicitly produce the equivalent water contents of six species of hydrometeors (cloud droplets, raindrops, graupel particles, pristine ice crystals, ice aggregates and snow flakes) as a function of space and time. From the outputs of the cloud models, the upwelling brightness temperatures are computed, and the corresponding hydrometeor equivalent liquid water content (LWC) profiles are extracted for the CRD.

[12] The simulated TBs are generated by means of a 3-D adjusted plane-parallel radiative transfer (RT) code [*Roberti et al.*, 1994; *Liu et al.*, 1996; *Bauer et al.*, 1998] at the TMI frequencies and viewing angle (53.1°). The TBs are computed at model resolution (which is generally much higher than the satellite footprints), and then spatially filtered in order to reach TMI effective resolutions for the different channels. At each frequency, the antenna pattern of the radiometer is simulated by means of a two-dimensional Gaussian weighting function, where the half-power beam width equals half the footprint at that frequency.

[13] In addition to the hydrometeor LWC profiles, the database contains the corresponding precipitation rate profiles for both rain and ice (i.e., graupel and snow). At each altitude, the rain and ice precipitation rate is computed by using the terminal fall velocities as in the work of *Mugnai et al.* [1993], but using the vertical wind speed, temperature and pressure produced by the cloud model, and the rain and ice size distributions used within the RT computations.

[14] As shown in Figure 1, a very important component of the algorithm is the error covariance matrix, which accounts for the TB sensitivity to the parameter uncertainties and/or approximations used within the CRD generation. In order to compute this matrix the various parameters used in the RT computations (e.g., drop size distributions, sea surface wind speed, presence of partially melted hydrometeors) have been perturbed with respect to the standard values used within the cloud model simulations, and the corresponding TB errors have been taken into account. From our preliminary analysis, we obtained values ranging from 3 K at 10 GHz to 8 K at 85 GHz.

2.1.2. Cloud and Radiative Transfer Models

[15] At present, we make use of two hurricane simulations (i.e., hurricane Gilbert and hurricane Bonnie) generated by the University of Wisconsin Nonhydrostatic Modeling System (UW-NMS) [*Tripoli*, 1992], and of a simulation of a tropical squall line observed during TOGA-COARE (hereafter, TOGA simulation), that has been produced by the Goddard Cumulus Ensemble (GCE) cloud modeling system [*Tao and Soong*, 1986].

[16] In the UW-NMS simulations, the hydrometeor size distributions are given by constant-slope inverse exponential distributions (see *Panegrossi et al.* [1998] for details about the model microphysics) with slopes equal to 1.852 mm^{-1} for rain, 2 mm^{-1} and 1 mm^{-1} for graupel (for hurricane Bonnie and for hurricane Gilbert, respectively), and 0.3 mm^{-1} for snow and aggregates. Cloud droplets and pristine ice crystals are monodispersed with diameters equal to 0.02 mm and 0.230 mm, respectively. Hydrometeor density is equal to 0.22 g/cm^3 and 0.6 g/cm^3 for ice crystals and graupel particles, respectively, while for snow and ice aggregates it varies with size as in *Panegrossi et al.* [1998]. For the GCE model, constant-intercept drop size distributions are assumed [*Kummerow et al.*, 1996], with intercepts equal to 8000 m^{-3} mm^{-1} for rain, and 4000 m^{-3} mm^{-1} for graupel, snow and aggregates. Graupel density is 0.4 g/cm^3, while snow density is 0.1 g/cm^3. Cloud droplets and cloud ice are monodispersed with diameters equal to 0.1 mm and 0.02 mm, respectively, and ice density is 0.9 g/cm^3.

[17] The upwelling microwave brightness temperatures that would be observed by the radiometer must be computed over the simulated satellite footprints. This can be achieved by means of one-dimensional (1-D) plane-parallel RT schemes, following two different ways having different physical meaning [*Kummerow et al.*, 1996]. In the first approach, which may be called ''1-D average-microphysics approach,'' the cloud model out-

puts within vertical cloud boxes corresponding to such satellite footprints are horizontally averaged in order to generate plane-parallel cloud structures at the resolution of the radiometer, to which a 1-D RT code is then applied. In the second approach, which may be called "1-D average-TB approach," the 1-D RT code is applied to plane-parallel cloud structures corresponding to the various cloud model columns; and the upwelling TBs are averaged over the cloud columns contained by the various satellite footprints. It turns out that, in general, the second approach performs better; i.e., the results are closer to corresponding TBs computed by means of 3-D Monte Carlo RT schemes [*Marzano et al.*, 2000]. Nevertheless, both approaches may produce large errors. That is why we have resorted to a 3-D backward Monte Carlo RT scheme [*Roberti et al.*, 1994] as well as to a 3-D adjusted plane parallel approach in which the plane-parallel cloud structures are generated from the cloud model paths along the radiometer direction of sight (i.e., at about 53°), rather than from the vertical cloud model columns. This approach gives quite good results because it overcomes the geometrical errors that a simple 1-D scheme is prone to [*Bauer et al.*, 1998; *Liu et al.*, 1996]. However, in cases of enhanced horizontal inhomogeneities it produces large discrepancies that must be taken into account within the error covariance estimation of retrieval scheme.

2.2. Coupling Cloud Radiation Databases and Bayesian Techniques

[18] Within the forward problem the radiative signatures of cloud model simulations have been simulated. However, this is not sufficient when the simulated brightness temperatures and corresponding profiles are to be used for inversion purposes [*Bauer*, 2001]. In fact, extreme care must be paid to the significance and the limitations of the database itself, the construction of which requires a number of additional information: error distributions, profile accuracy, range of applicability of the database within different meteorological conditions (needed in order to provide a valuable tool for statistical inversions on a wide range of meteorological cases). Also, attention must be paid in defining the trade-off between two opposite needs: inversion-oriented databases in fact must be not too large (for computer efficiency problems) but as complete as possible (in order to account for as much as possible situations). This means that the manifold of the simulated TBs must be "statistically significant" and representative of the meteorological event under investigation.

2.2.1. Matching Between Observations and Measurements

[19] Before performing the retrieval, it is necessary to check the capability of the database in reproducing the event under consideration from a radiative point of view [*Marzano et al.*, 2000; *Bauer*, 2001]. On a rigorous basis, a retrieval based on a pregenerated database may be performed only if the manifold of the measured TBs is completely overlapped by that of the simulations. On the contrary, when the two manifolds are largely different, the precipitation event is not adequately represented by the database [*Panegrossi et al.*, 1998] and therefore no retrieval should be attempted.

[20] The agreement between the observed and simulated manifolds is quantified by means of an ad hoc Database Matching Index (DMI), which expresses the percentage of the observed TB pixels which have at least one simulated point closer than a given threshold in the multidimensional space of the simulated TBs. This threshold is given by the error covariance matrix, which is the output of the error covariance estimator indicated in Figure 1, and takes into account all modeling as well as instrumental errors. In summary, when generating a CRD, one should choose the minimum DMI allowed for a given set of reference cases. The density of database TBs can be decreased until the minimum DMI value is reached. In the present work, we have expanded the database until obtaining DMI $\geq$95% for all case studies.

2.2.2. Profile Characterization in a 3-D Approach

[21] A key point of the CRD generation concerns the definition of the cloud structures, which have to be associated with the simulated TBs. As described in the previous section, TBs are computed along slanted columns at model resolution, and then averaged over the simulated scenario according to the size of the footprints at the various TMI frequencies. Table 1 shows the number of pixels, which are averaged to match TMI resolutions for every simulation. Considering that the three cloud model simulations have different horizontal resolutions (i.e., 2.5 km, 3.3 km, and 1.0 km for hurricane Bonnie, hurricane Gilbert, and TOGA, respectively), which are much higher than the resolution of the TMI channels, a different number of pixels has been considered to uniquely identify the cloud structure associated with each set of simulated TBs. Notice that this number may be fractions of model pixels: in order to reach TMI resolutions with a larger accuracy, a subpixel domain has been considered as in the spatial filtering described in section 2.1.

[22] In principle, for each TMI frequency a different cloud structure (filling up the slanted elliptical cylinder with sizes corresponding to the cross-track and along-track resolutions of each frequency) should be associated with each TB point of the database. This problem could be faced by associating a cloud structure contained in a sort of deformed elliptical cylinder, having horizontal sizes that vary with height according to the frequency-dependent contribution of each cloud layer to the upwelling TBs. This strategy, however, would be rather

Table 1. Number of Model Pixels Required to Match TMI Fields of View (FOVs) at 10, 19, 37 and 85 GHz Using the Three Available Simulations (i.e., Bonnie, Gilbert, and TOGA), Used to Generate the Cloud Radiation Database[a]

	10 GHz	19 GHz	37 GHz	85 GHz
TMI, km	59 × 35.7	30 × 18	16 × 9.7	6.9 × 4.2
Bonnie, pixels	24 × 14	12 × 7	6 × 4	3 × 2
Gilbert, pixels	18 × 11	9 × 6	5 × 3	2 × 1
TOGA, pixels	59 × 36	30 × 18	16 × 10	7 × 4

[a]TMI FOVs are listed at the first row.

complex and pixel-dependent. The simplest choice is therefore to choose a common single resolution for the retrieved products belonging to the CRD.

[23] Within BAMPR we have associated slanted cloud structures corresponding to the resolution of the 37 GHz frequency as a reasonable compromise, which is considered to be optimal with respect to TMI sampling characteristics as well. In order to characterize the retrieval error, intrinsic to the choice of a single-resolution cloud structure, we have also taken into account the variability (both in terms of cloud profiles and simulated TBs) of the 37 GHz inside the footprints of the 19 and 10 GHz, as well as of the 85 GHz inside the 37 GHz footprint. This beam-filling evaluation is part of the error covariance estimator, introduced in Figure 1 [*Tassa et al.*, 1999; *Marzano et al.*, 2000]. The previous discussion also evidences that, when using a 3-D approach, the performances of the retrieval depend on the cloud model capability to reproduce not only the microphysics of the simulated events, but also their horizontal patterns and spatial features.

2.2.3. Representativeness of the Database

[24] As already mentioned, a pregenerated database should be able to simulate different typologies of events (and, possibly, several events for each typology) to generate a global database, which can be successfully applied to the various precipitation regimes. An interesting analysis concerns the identification of the portions of the database that are used by the algorithm for the retrieval of different events.

[25] In order to evaluate the representativeness of the various cloud model simulations, we have introduced the Database Index (DBI) to quantify the relative occurrence of each simulation within the retrieval process. For simplicity, we have defined DBI as the index referring to the CRD (derived from Bonnie, Gilbert and TOGA simulations), which generates the closest set of TBs with respect to each TMI measurement.

[26] Figure 2 shows the results of this analysis for three case studies, that is the hurricane Bonnie (TRMM data granule 4267), a tropical storm called Astrid (TRMM data granule 11938) and a tropical front (TRMM data granule 17455) by using different symbols for DBI. From the analysis of the figure, it emerges that, as expected for the intense core of the cyclones, the algorithm selects cloud structures provided by the two hurricane simulations, whereas on the cloud edges and for narrow cells the TOGA simulation is preferred.

[27] Table 2, which gives DBI values referred to Figure 2, confirms that for the hurricane case almost 80% of the retrieved profiles are taken from the hurricane simulations, whereas the other two cases both show an opposite trend, taking 57% of the samples out from the TOGA simulation. Note that simulated upwelling TBs depend not only on the hydrometeor profiles (which are different for the three simulations), but also on the different beam filling characterization of the simulations.

2.3. The Inverse Problem

[28] The BAMPR technique, like almost all rainfall estimation techniques, adopts a probabilistic approach due to the statistical nature of precipitating cloud parameters. The MMS method, used within BAMPR retrieval scheme, will be outlined in the following section.

2.3.1. BAMPR Retrieval Method

[29] The inversion scheme for BAMPR is shown on the left side of Figure 1. As a first step, over-land and coastal pixels are screened away, together with the clear sky pixels over ocean. The rain detection is based upon the measured TBs using the same method of the TMI official algorithms [*Kummerow et al.*, 1998]. The second phase concerns the identification of the rainfall regime, which is achieved by determining if the measured TBs belong to either the moderate or to the intense rainfall class of the CRD (as it is detailed in the following section). In the third step, the Bayesian MMS inversion algorithm is applied using only the selected class of the CRD. Output products are the hydrometeor and/or precipitation rate profiles, together with columnar LWCs and surface rain rates.

[30] Within the MMS Bayesian criterion, the hydrometeor profile estimate is given by the expected value of the hydrometeor profiles conditioned to the spaceborne measured multifrequency TB, i.e., it is practically an ensemble weighted average of the hydrometeor profiles (belonging to the selected CRD) whose radiative signatures lie around the observed TBs. The MMS approach helps in overcoming some stability problems due to the numerical implementation of the Maximum A posteriori Probability (MAP) algorithm [*Marzano et al.*, 1999].

[31] If we indicate with $\mathbf{g}$ the geophysical (hydrometeor content) vector related to a profile set of the CRD and with $\mathbf{t}_m$ the multispectral vector of TMI measurements, the MMS estimate $\hat{\mathbf{g}}_{\mathbf{MMS}}$ is defined as the expected value of $\mathbf{g}$, given a set of measurements $\mathbf{t}_m$, i.e.,

$$\hat{\mathbf{g}}_{\mathrm{MMS}} = \langle (\mathbf{g}|\mathbf{t}_m) \rangle, \tag{1}$$

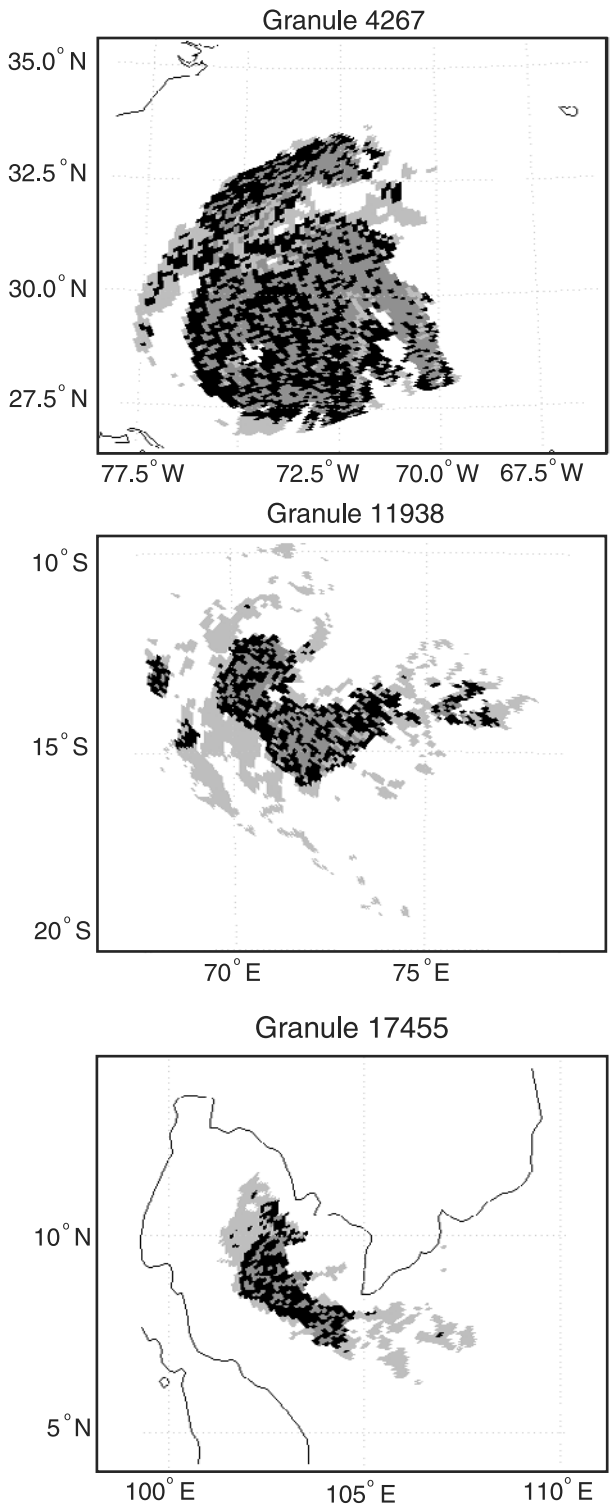

Figure 2. (opposite) Maps of Database Indexes (DBI) for hurricane Bonnie on 25 August 1998 (granule 4267, top panel), tropical storm Astrid on 24 December 1999 (granule 11938, middle panel) and a tropical oceanic front occurred on 8 December 2000 (granule 17455, bottom panel). The gray-to-black pixels represent only rainy pixels over ocean surfaces. The different shaded pixels identify DBIs for hurricane Bonnie (black), hurricane Gilbert (dark gray), and TOGA (light gray) simulations.

Table 2. Results for the Database Index (DBI), Given in Percentage and Associated With the Bonnie, Gilbert, and TOGA CRDs, for Three TMI Case Studies Referred to Hurricane Bonnie (Data Granule 4267), a Tropical Storm Called Astrid (data granule 11938), and a Tropical Front (Data Granule 17455)[a]

		Cloud Radiation Database		
		Bonnie, %	Gilbert, %	TOGA, %
TRMM data	Bonnie (Granule 4267)	47	31	22
	Astrid (Granule 11938)	30	13	57
	Front (Granule 17455)	31	12	57

[a]Only rainy pixels are considered.

where the angle brackets indicate an ensemble averaging with respect to $\mathbf{g}$. Equation (1) can be given in an explicit form as

$$\hat{\mathbf{g}}_{\mathrm{MMS}} = \int_0^\infty \mathbf{g}\, p(\mathbf{g}|\mathbf{t}_m) d\mathbf{g}, \tag{2}$$

where $p(\mathbf{g}|\mathbf{t}_m)$ is the conditional probability density function (PDF) of $\mathbf{g}$. It is important to remark that the MMS algorithm can easily furnish a measure of its intrinsic accuracy since it can be proved that

$$\boldsymbol{\sigma}^2_{\mathrm{gMMS}} = \left\langle [(\mathbf{g}|\mathbf{t}_m) - \hat{\mathbf{g}}_{\mathrm{MMS}}]^2 \right\rangle, \tag{3}$$

where $\boldsymbol{\sigma}^2_{\mathrm{gMMS}}$ is the variance vector of the estimated profile $\hat{\mathbf{g}}_{\mathbf{MMS}}$. The MMS algorithm is also referred to as the Minimum Variance algorithm because it corresponds to minimize the conditional variance of $\mathbf{g}$ given $\mathbf{t}_m$ [*Marzano et al.*, 2000].

[32] Using the Bayes theorem, $p(\mathbf{g}|\mathbf{t}_m)$ can be transformed in the following way:

$$\begin{aligned} p(\mathbf{g}|\mathbf{t}_m) &= p(\mathbf{t}_m|\mathbf{g})p(\mathbf{g})/p(\mathbf{t}_m) \\ &= p[\boldsymbol{\varepsilon}_t(\mathbf{g})]p(\mathbf{g})/p(\mathbf{t}_m), \end{aligned} \tag{4}$$

where $p(\mathbf{g})$ is the a priori PDF due to $\mathbf{g}$, and $\varepsilon_t(g) = [\mathbf{t}(\mathbf{g}) - \mathbf{t}_m]$ is the TB error vector with $\mathbf{t}(\mathbf{g})$ the simulated TB vector, related to $\mathbf{g}$ through the radiative transfer model. Equation

(4) puts in evidence the TB error ε_t, which takes into account not only the radiometric absolute accuracy, but also other possible sources of error due to the forward modeling [*Kummerow et al.*, 1996; *Marzano et al.*, 1999].

[33] The implementation of equation (2) can be carried out by noting that, since the CRD (CRD) consists of a discrete number of profiles (N_{CRD}), the available PDFs are not continuous functions, unless we choose analytical expressions. While a Gaussian distribution for $p[\varepsilon_t(\mathbf{g})]$ is reasonable, any assumption on $p(\mathbf{g})$ can be very often unrealistic. The probability density functions $p(\mathbf{g})$ for each profile may be approximated as

$$p(\mathbf{g}) \sim h(\mathbf{g}, \Delta\mathbf{g}), \tag{5}$$

where $h(\mathbf{g}, \Delta\mathbf{g})$ is the histogram relative to the sample $\mathbf{g}$ within a variable bin $\Delta\mathbf{g}$. Thus the *i*-th element $\mathbf{g}(i)$ of the hydrometeor profile $\mathbf{g}$ can be estimated as follows:

$$\hat{\mathbf{g}}_{MMS}(i) = k \sum_{j=1}^{N_{CRD}} g_j(i) e^{-0.5\left(\mathbf{t}(\mathbf{g}_j)-\mathbf{t}_m\right)^T \mathbf{C}_{\varepsilon_t}^{-1}\left(\mathbf{t}(\mathbf{g}_j)-\mathbf{t}_m\right)} \cdot h\left(g_j(i), \Delta\mathbf{g}_j\right), \tag{6}$$

where $\mathbf{g}_j$ is the *j*-th sample of the CRD, $\mathbf{t}(\mathbf{g}_j)$ is the corresponding TB, and $\mathbf{C}_{\varepsilon t}$ is the error covariance matrix. The constant *k* is such that

$$\sum_{j=1}^{N_{CRD}} e^{-0.5\left(\mathbf{t}(\mathbf{g}_j)-\mathbf{t}_m\right)^T \mathbf{C}_{\varepsilon_t}^{-1}\left(\mathbf{t}(\mathbf{g}_j)-\mathbf{t}_m\right)} h\left(g_j(i), \Delta\mathbf{g}_j\right) = 1. \tag{7}$$

2.3.2. Rainfall Classification and Estimate Uncertainty

[34] As shown in Figure 1, the database of the simulated TBs is clustered into two separate classes corresponding to moderate and intense precipitation regimes. This classification, which partially mitigates the ill-conditioning of the problem and is also useful for speeding up the retrieval, is unsupervised and based on the upwelling TBs and the 85 GHz spatial standard deviation and correlation within the 37 GHz FOV window [*Marzano et al.*, 2000]. This approach is similar to those available in literature [see, e.g., *Hong et al.*, 1999].

[35] The choice to avoid a more classical discrimination between stratiform and convective profiles (instead of moderate and intense) is justified by the fact that such criterion is hardly applicable over slanted cloud profiles (see section 2.1), because mixed convective and stratiform portions often coexist within the same cloud structure. The use of the spatial information has shown to be crucial for distinguishing narrow, but intense cells and for overcoming the beam-filling problems intrinsic to the poor resolution of the TMI 10 GHz channel.

[36] The strong nonlinearity of the forward problem implies a nonuniqueness feature of the inverse problem so that very different microphysical structures can produce similar TB vectors. As mentioned, a remarkable feature of BAMPR is that each estimate is accompanied by its relative uncertainty [*Marzano et al.*, 2000; *Bauer et al.*, 2001]. The MMS algorithm can provide a measure of this inherent uncertainty, which can be computed according to equation (3). The amount of this uncertainty depends on the capability of the cloud radiative model simulation to reproduce the spatial structure and dynamical range of the upwelling radiation, as well as on the typology of the meteorological event observed. It is worth noticing that the database classification into moderate and intense rain regimes plays an important role in this regard as it reduces the inherent dispersion of cloud profiles associated with a given TB vector.

[37] Figure 3 shows the relative uncertainty (as percentage with respect to the corresponding estimate, as described in section 2.3) of the surface rainfall rates, estimated by BAMPR for three TRMM overpasses during the three case studies mentioned in Table 2. For all three cases the impact of the uncertainties is extremely large at light rainfall rates (below 2 mm/h), but it tends to rapidly decrease for increasing rain rates, leveling off in correspondence of the most intense rain pixels. Remarkably, this tendency is much more evident for the case of hurricane Bonnie which is characterized by lower, less scattered values, and stabilizes at about 50–60% for rain rates larger than 15 mm/h. This may be due to the fact that the CRD contains two hurricane simulations, so that the radiative appearance of the hurricane is better represented. The uncertainties could be reduced, for instance, by an improved classification of rain regimes and event typology, which would diminish the dispersion of the cloud profiles associated with similar TBs.

3. Application to TRMM Data

[38] Before applying BAMPR to a case study, it may be useful to summarize its standard products which are basically: (1) surface rainfall rates (in mm/h); (2) precipitation rate profiles (in mm/h) for both precipitating liquid (rain) and ice (snow and graupel); (3) equivalent water-content columnars (in kg/m^2) and profiles (in g/m^3) for six different hydrometeors (i.e., cloud water, rain, graupel, cloud ice, snowflakes, and ice aggregates). The estimated profiles are slanted (at TMI viewing angle), at the resolution of the 37 GHz (i.e., 15 × 13 km) and characterized by the corresponding estimate uncertainties as well.

3.1. Case Study of Hurricane Bonnie

[39] BAMPR has been applied and tested over different types of events: a tropical cyclone (hurricane Bonnie), a tropical storm (called Astrid), a tropical front and some sparse convective cells in the Atolls region have

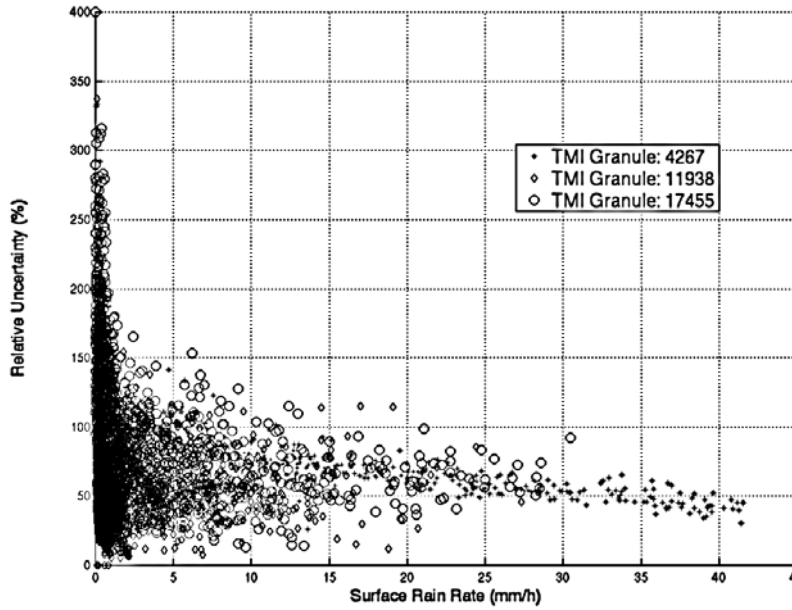

Figure 3. Rainfall rate normalized uncertainties (defined as the ratio in percentage between estimate standard deviation and estimated value) of BAMPR algorithm versus surface rain rate estimates, for TMI observations of the three case studies of Figure 2.

been analyzed [*Bauer et al.*, 2001]. Special attention has been paid to the case of hurricane Bonnie, due to the fact that the CRD contains a dedicated simulation. This case provided the best results when compared to the PR measurements, while the largest differences have been observed for the Atolls cases.

[40] In what follows we will focus on the TMI data granule 4267, which corresponds to 25 August 1998 when TRMM passed over hurricane Bonnie in the most intense period of the cyclone evolution. Figure 4 shows the central pixels of the TMI swath in the along-track direction at 10, 19, 37 and 85 GHz and the corresponding nadir-looking measured PR reflectivities along the nadir section (delay time between TMI and PR has been disregarded here). In panel a), the maxima of the TBs at 10 and 19 GHz indicate the presence of large amounts of liquid water in the low-to-mid layers of the precipitating cloud, while the minima at 37 and especially at 85 GHz correspond to scattering cooling due to large amounts of high-density frozen particles aloft (for a thorough discussion about the sensitivity of the various TMI channels to the cloud microphysics, see, e.g., *Mugnai et al.* [1993]).

[41] The observed scene is fairly composite with a strong updraft embedded within a large stratiform region around 600 km in the along-track direction. This case is really peculiar because of the pronounced tilting of the convective tower, evidenced by the 10 km shift between the corresponding PR reflectivity peak and the TB deep minimum at 85 GHz (see *Hong et al.* [2000] for more details on the interpretation of these measurements). Also noteworthy is that the various TMI measurements at the different frequencies are shifted with respect to each other.

3.2. Results

[42] Figure 5 shows BAMPR-estimated surface rainfall rates corresponding to the measured brightness temperatures of Figure 4. These estimates are shown together with the relative uncertainties (indicated by error bars) and compared with NASA's official TMI-derived rainfall estimates; i.e., "2A12" product, version 5. This product is obtained by using the Goddard Profiling Algorithm (GPROF), described by *Kummerow et al.* [2001]. Systematic higher values of 2A12 estimates with respect to BAMPR ones are evident. In addition, there is a slight displacement of the rainfall peak around 600 km, which seems to be associated with the shift between the measured TBs, pointed out in Figure 4. While the 2A12 estimates appear to be more related to the 85 GHz measurements, the BAMPR estimates tend to follow the TB behavior of TMI lower frequencies.

[43] These results reflect the differences between the two algorithms, which concern both the implementation

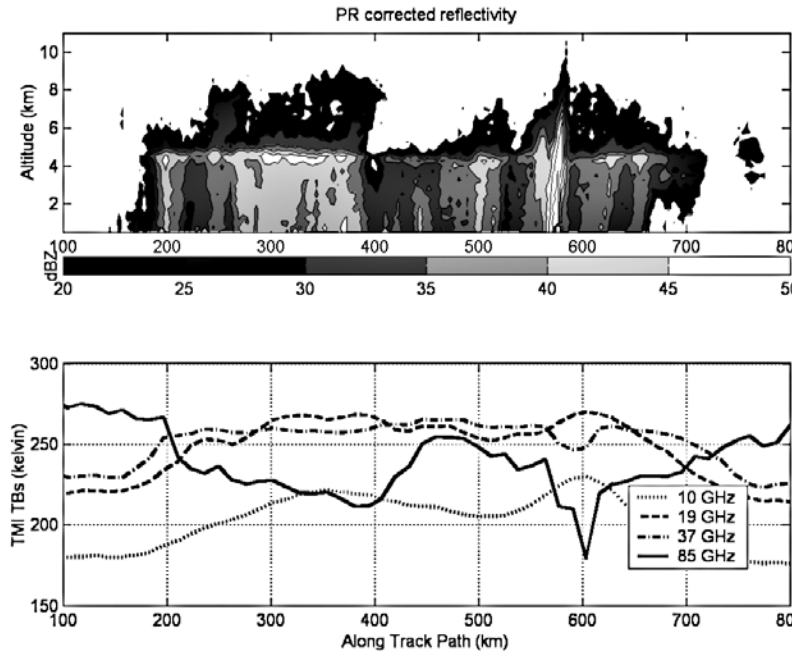

Figure 4. Nadir-looking section of PR measured reflectivities (upper panel) and along-track TMI brightness temperatures at swath center (lower panel) for hurricane Bonnie on 25 August 1998 (granule 4267).

of the Bayesian inversion as well as the generation of the CRD (in spite of the use of the same cloud model simulations). In particular, we notice that the 3-D approach, used within BAMPR for the generation of the CRD, could be the main reason for the weaker correlation of BAMPR estimates with the higher frequency TBs (that is, the use of slanted profiles implies weaker correlations between ice aloft and rainwater contents) therefore explaining the shift in the rainfall peaks. This difference, however, might only partially justify the BAMPR lower values, which could depend also on other factors such as the selected cloud model simulation, the rainfall classification, the drop size distributions and the product spatial resolution.

[44] In spite of these differences, the two estimates are still highly correlated: we obtained a correlation coefficient of 0.8 for the considered track and 0.7 for the whole case; a value which is one of the highest obtained for the cases under investigation (which range from 0.45 for the Atolls cases to 0.7 for other hurricanes).

[45] Since BAMPR produces precipitation rate profiles, the comparison with PR products can be accomplished at several altitudes. This comparison is fairly cumbersome due to the differences intrinsic in the two instruments and therefore in the two estimates. The radar-derived profiles are nearly vertical and have higher vertical and horizontal resolutions (250 m and 4×4 km, respectively), while BAMPR estimates are slanted and have much lower resolutions (from 500 m to 1.5 km and 13×15 km, respectively). The problem of this intercomparison has been tackled by degrading the resolution of TRMM official products for PR (''2A25'' products; see *Iguchi et al.* [2000]) both horizontally and vertically by interpolating and averaging both 2A25 and BAMPR estimates into five layers: 1.0–2.5 km; 2.5–4.0 km; 4.0–5.5 km; 5.5–7 km; and above 7 km. Note that the effect of different inclinations between PR and BAMPR estimates has not been corrected since the displacement below 10 km of retrieved cloud structures is almost negligible at BAMPR product resolution.

[46] In Figure 6 BAMPR estimates are shown together with the corresponding PR estimates for the four lower layers. The most remarkable feature is that the rainfall peaks are quasi collocated, while the rainfall rate produced by the convective tower is underestimated by BAMPR. In the stratiform region, PR products are almost always lower than BAMPR's, even though they remain within BAMPR estimation uncertainty. Finally, even though the convective portion of the cross section is underestimated, BAMPR surface rainfall rates tend to be in between 2A12 and 2A25 estimates, thus reducing

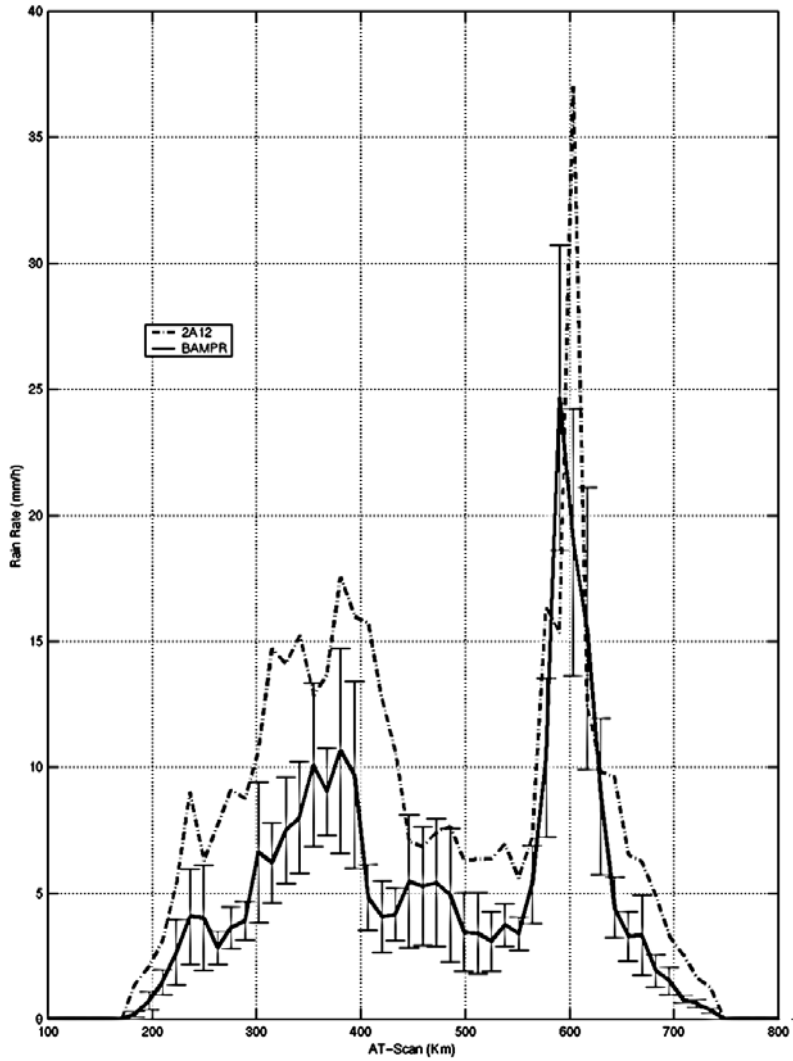

Figure 5. BAMPR surface rainfall rate estimates together with 2A12 estimates, derived from TMI data shown in Figure 4. Error bars represent BAMPR estimation uncertainty (in terms of standard deviation).

the gap between the two official products documented also by *Kummerow et al.* [2001].

4. Conclusions

[47] The methodological features of a Bayesian inversion method (BAMPR), trained by 3-D cloud-resolving models combined with 3-D radiative transfer models, have been extensively investigated. The forward problem has been discussed in detail, pointing out the fact that much attention should be paid in the generation of the CRD. In particular, we found it useful to introduce two dedicated indices in order to quantify the potential of the database in representing the meteorological event under investigation. The modeling assumptions may bring some errors and limitations, which are taken into account by the retrieval algorithm through a model covariance estimator. Finally, by choosing a MMS Bayesian approach, BAMPR can provide a measure of the internal estimate uncertainty in terms of error covariance for each product.

[48] The BAMPR algorithm has been applied and tested over several TRMM cases. Comparisons with

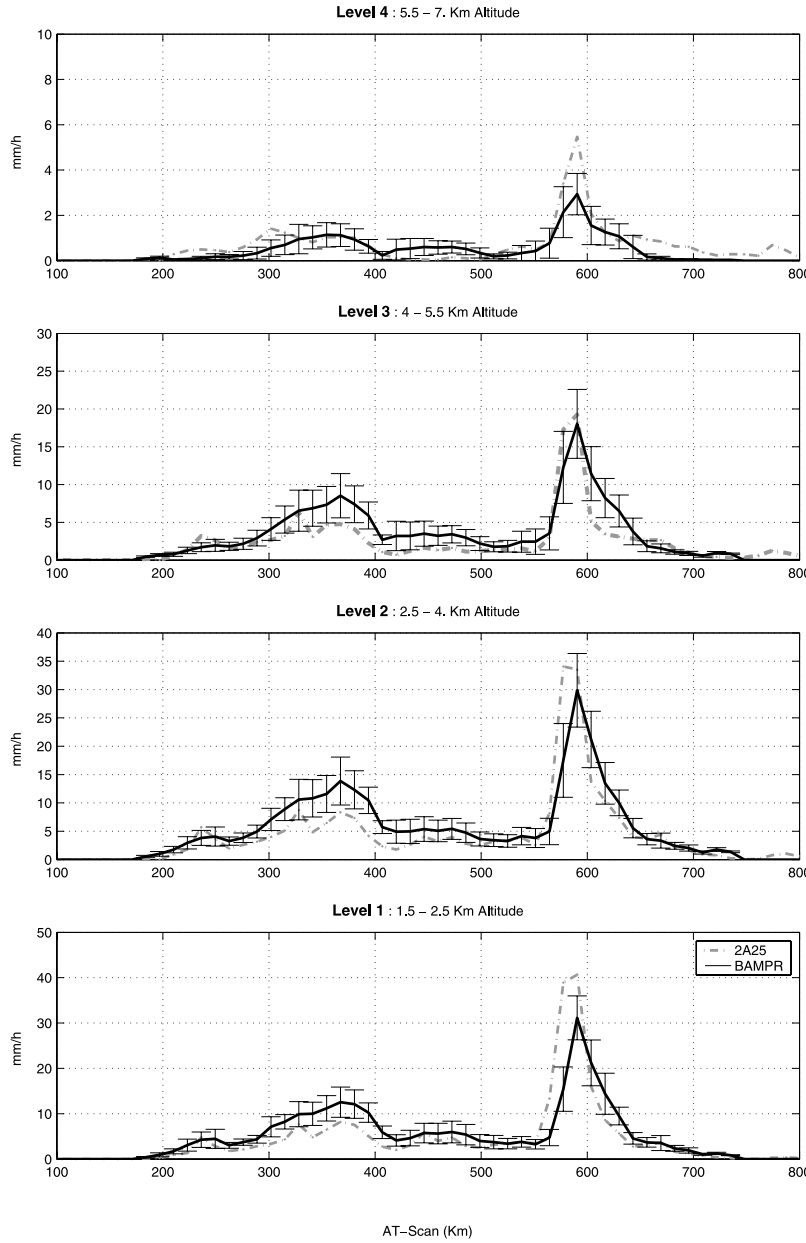

Figure 6. BAMPR rain precipitation rate estimates for the layers 1.5–2.5 km, 2.5–4 km, 4–5.5 km and 5.5–7 km. Black solid lines with associated error bars indicate BAMPR estimates with their corresponding uncertainties, while dashed lines correspond to the spatially averaged PR 2A25 estimates (as in Figure 4).

TRMM official estimates indicate a general underestimation of BAMPR versus the official TMI-only products, with correlation factors ranging from 0.45 to 0.7 for all cases under examination. In particular, the case of the hurricane Bonnie on 25 August 1998 has been analyzed in detail. It turns out that the estimated precipitation rate profiles tend to be in reasonably good agreement with PR official products, and that the surface rainfall rates in the stratiform region are in between those estimated by the PR and TMI official algorithms.

[49] **Acknowledgments.** This work has been supported by the European Commission through the EuroTRMM project (1997–2000), by the Italian National Group for Prevention from Hydrological Hazards (GNDCI), by the Italian Space Agency (ASI) and by the European Space Agency (ESA). We wish to thank Gregory Tripoli and Giulia Panegrossi of the University of Wisconsin for providing the hurricane Bonnie simulation and for profitable interactions.

References

Bauer, P., Over-ocean rainfall retrieval from multi-sensor data of Tropical Rainfall Measuring Mission (TRMM), part I: Design and evaluation of inversion databases, *J. Oceanic Atmos. Technol.*, *18*, 1315–1330, 2001.

Bauer, P., L. Schanz, and L. Roberti, Correction of the three-dimensional effects for passive microwave remote sensing of convective clouds, *J. Appl. Meteorol.*, *37*, 1619–1632, 1998.

Bauer, P., J. F. Mafhouf, W. S. Olson, F. S. Marzano, S. Di Michele, A. Tassa, and A. Mugnai, Error analysis in rainfall retrieval for variational data assimilation, *Q. J. R. Meteorol. Soc.*, *127*, 1–26, 2001.

Di Michele, S., F. S. Marzano, A. Mugnai, A. Tassa, and J. P. V. Poiares Baptista, Physically-based statistical integration of TRMM microwave measurements for precipitation profiling, *Radio Sci.*, *38*, doi:10.1029/2002RS002636, in press, 2003.

Evans, K. F., J. Turk, T. Wong, and G. L. Stephens, A Bayesian approach to microwave precipitation profile retrieval, *J. Appl. Meteorol.*, *34*, 260–279, 1995.

Hong, Y., C. Kummerow, and W. S. Olson, Separation of convective and stratiform precipitation using microwave brightness temperatures, *J. Appl. Meteorol.*, *38*, 1195–1213, 1999.

Hong, Y., J. Hafermann, W. S. Olson, and C. Kummerow, Microwave brightness temperatures from tilted convective systems, *J. Appl. Meteorol.*, *39*, 983–998, 2000.

Iguchi, T., R. Meneghini, J. Awaka, T. Kozu, and K. Okamoto, Rain profiling algorithm for TRMM precipitation radar data, *Remote Sens. Appl. Earth Atmos. Ocean*, *25*, 973–976, 2000.

Kummerow, C., W. S. Olson, and L. Giglio, A simplified scheme for obtaining precipitation and vertical hydrometeor profiles from passive microwave sensors, *IEEE Trans. Geosci. Remote Sens.*, *34*, 1213–1232, 1996.

Kummerow, C., W. Barnes, T. Kozu, J. Shiue, and J. Simpson, The Tropical Rainfall Measuring Mission (TRMM) sensor package, *J. Atmos. Oceanic Technol.*, *15*, 809–817, 1998.

Kummerow, C., D. B. Shin, Y. Hong, W. S. Olson, S. Yang, R. F. Adler, J. McCollum, R. Ferraro, G. Petty, and T. T. Wilheit, The evolution of the Goddard Profiling algorithm (GPROF) for rainfall estimation from passive microwave sensors, *J. Appl. Meteorol.*, *40*, 1801–1820, 2001.

Liu, Q., C. Simmer, and E. Ruprecht, Three-dimensional radiative transfer effects of clouds in the microwave spectral range, *J. Geophys. Res.*, *101*, 4289–4298, 1996.

Marzano, F. S., A. Mugnai, G. Panegrossi, N. Pierdicca, E. A. Smith, and J. Turk, Bayesian estimation of precipitating cloud parameters from combined measurements of spaceborne microwave radiometer and radar, *IEEE Trans. Geosci. Remote Sens.*, *37*, 596–613, 1999.

Marzano, F. S., S. Di Michele, A. Tassa, and A. Mugnai, Bayesian techniques for precipitation profiles retrieval from spaceborne microwave radiometers, in *Proceedings of PORSEC-2000*, pp. 221–228, Indian Natl. Inst. of Oceanogr., Goa, India, Dec. 2000.

Mugnai, A., E. A. Smith, and G. J. Tripoli, Foundations for statistical-physical precipitation retrieval from passive microwave satellite measurements, part II: Emission source and generalized weighting function properties of a time dependent cloud radiation model, *J. Appl. Meteorol.*, *32*, 17–39, 1993.

Panegrossi, G., S. Dietrich, F. S. Marzano, A. Mugnai, E. A. Smith, X. Xiang, G. J. Tripoli, P. K. Wang, and J. P. V. Poiares Baptista, Use of cloud model microphysics for passive microwave-based precipitation retrieval: Significance of consistency between model and measurement manifolds, *J. Atmos. Sci.*, *55*, 1644–1673, 1998.

Pierdicca, N., F. S. Marzano, G. D'Auria, P. Basili, P. Ciotti, and A. Mugnai, Precipitation retrieval from spaceborne microwave radiometers using maximum a posteriori probability estimation, *IEEE Trans. Geosci. Remote Sens.*, *34*, 831–845, 1996.

Roberti, L., J. Haferman, and C. Kummerow, Microwave radiative transfer through horizontally inhomogeneous precipitating clouds, *J. Geophys. Res.*, *99*, 16,707–16,718, 1994.

Simpson, J., C. Kummerow, W. K. Tao, and R. F. Adler, On the Tropical Rainfall Measuring Mission (TRMM), *Meteorol. Atmos. Phys.*, *60*, 19–36, 1996.

Smith, E. A., A. Mugnai, H. J. Cooper, G. J. Tripoli, and X. Xiang, Foundations for statistical-physical precipitation retrieval from passive microwave satellite measurements, part I: Brightness-temperature properties of a time-dependent cloud-radiation model, *J. Appl. Meteorol.*, *31*, 506–531, 1992.

Smith, E. A., X. Xiang, A. Mugnai, and G. J. Tripoli, Design of an inversion-based precipitation profile retrieval algorithm using an explicit cloud model for initial guess microphysics, *Meteorol. Atmos. Phys.*, *54*, 53–78, 1994.

Smith, E. A., et al., Results of WetNet PIP-2 projects, *J. Atmos. Sci.*, *55*, 1483–1536, 1998.

Tao, W. K., and S. T. Soong, A study of the response of deep tropical clouds to mesoscale processes: Three dimensional numerical experiments, *J. Atmos. Sci.*, *43*, 2653–2676, 1986.

Tassa, A., S. Di Michele, E. D'Acunzo, C. Accadia, S. Dietrich, A. Mugnai, F. Marzano, G. Panegrossi, and L. Roberti, Analysis of TRMM observations of heavy precipitation events, in *Microwave Radiometry and Remote Sensing of*

the Earth's Surface and Atmosphere, edited by P. Pampaloni and S. Paloscia, pp. 371–377, VSP Int. Sci. Publ., Utrecht, Netherlands, 1999.

Tripoli, G. J., An explicit three-dimensional non-hydrostatic numerical simulation of a tropical cyclone, *Meteorol. Atmos. Phys.*, *49*, 229–254, 1992.

F. S. Marzano, Dipartimento di Ingegneria Elettrica, Center of Excellence on Remote Sensing and Hydrometeorology, Università dell'Aquila, Monteluco di Roio, L'Aquila, Italy. (marzano@ing.univaq.it)

S. Di Michele, A. Mugnai, and A. Tassa, Istituto di Scienze dell'Atmosfera e del Clima, Consiglio Nazionale delle Ricerche, Via del Fosso del Cavaliere, 100-00133 Rome, Italy. (s.dimichele@isac.cnr.it; a.mugnai@isac.cnr.it; a.tassa@isac.cnr.it)

J. P. V. Poiares Baptista, European Space Research and Technology Centre, European Space Agency, Noordwjik, Netherlands. (Pedro.Baptista@esa.int)